Bioorganic Chemistry 86 (2019) 569–582

Contents lists available at ScienceDirect

Bioorganic Chemistry

journal homepage: www.elsevier.com/locate/bioorg

Discovery of the Biginelli hybrids as novel caspase-9 activators in apoptotic machines: Lipophilicity, molecular docking study, influence on angiogenesis gene and miR-21 expression levels

Nenad Janković[a,*], Jovana Trifunović Ristovski[b], Milan Vraneš[c], Aleksandar Tot[c], Jelena Petronijević[a], Nenad Joksimović[a], Tatjana Stanojković[d], Marija Đorđić Crnogorac[d], Nina Petrović[d,e], Ivana Boljević[d], Ivana Z. Matić[d], Goran A. Bogdanović[e], Momir Mikov[b], Zorica Bugarčić[a]

[a] Department of Chemistry, Faculty of Science, University of Kragujevac, Radoja Domanovića 12, 34000 Kragujevac, Serbia
[b] Department of Pharmacology, Toxicology and Clinical Pharmacology, Faculty of Medicine, University of Novi Sad, Hajduk Veljkova 3, 21000 Novi Sad, Serbia
[c] Department of Chemistry, Biochemistry and Environmental Protection, University of Novi Sad, Trg Dositeja Obradovića 3, 21000 Novi Sad, Serbia
[d] Institute for Oncology and Radiology of Serbia, Pasterova 14, 11000 Belgrade, Serbia
[e] Vinča Institute of Nuclear Science, University of Belgrade, P.O. Box 522, 11001 Belgrade, Serbia

ARTICLE INFO

Keywords:
Biginelli scaffold
Selectivity index
Apoptosis
Caspase-9
Lipophilicity

ABSTRACT

In order to investigate potential therapeutically agents, novel products of Biginelli reaction (**4a-l**) were synthesized and exposed to cytotoxic and caspase activities, angiogenesis, cell cycle distribution, gene and microRNA expression levels, lipophilicity assessment and docking study. Among the twelve novel compounds (**4a-l**) evaluated for the cytotoxic activity, five of them (**4c**, **4d**, **4f**, **4k** and **4l**) that showed excellent activity on the tested cell lines (HeLa, LS174 and A549) were selected for further evaluation. Interestingly, compound **4f** has up to three times higher selectivity index (SI) towards cancer cells than cisplatin (on HeLa, LS174 and A549 SI = 18.2, 13.5 and 11.2, respectively). The obtained results from cell cycle distribution and caspase activity indicate that tested compounds (**4c**, **4d**, **4f**, **4k** and **4l**) promoted caspase-9 activation, implicated in the intrinsic pathway of apoptosis. Lipophilicity of **4a-l** was determinate by using reversed-phase high-performance liquid chromatography.

1. Introduction

2-oxo-1,2,3,4-tetrahydropyrimidines-THPMs (Fig. 1, former name is 3,4-dihydropyrimidin-2(1*H*)-ones-DHPMs) are an important class of heterocyclic compounds known for their broad spectrum of biological activities such as anti-HIV, antibacterial, antifungal, anti-tubercular, antioxidant, anti-inflammatory, anticancer, and also as potential agents in treatment of many diseases such as Alzheimer's disease, diabetes and other neuros diseases [1–5].

Nowadays one of the primary goals in medicine and one of the biggest problems in our society is cancer. Platinum-based drugs were the first agents that have been used in chemotherapy, and since then these drugs have been in the center of researches as chemotherapeutic agents [6,7]. Limited applicability and several side effects such as neurotoxicity, nephrotoxicity limited the use of cisplatin in cancer therapy [8–10], so the significant interests in medicinal chemistry are to develop new non-platinum-based drug with improved properties [11]. A wide variety of other metallodrugs [12–22] and non-metal drugs [23–27] were intensively studied as potential platinum replacements. The growing interest in the three-component reaction between an aldehyde, β-keto ester and urea or thiourea, that gives THPMs known as Biginelli reaction, is primarily due to the therapeutic and pharmacological properties of Biginelli products, namely, THPMs. Biginelli products are promising compounds for the treatment of cancer and the most investigated compound from this group, monastrol, was found to interrupt mitosis by inhibiting the motor activity of the kinesin Eg5, a protein involved in spindle bipolarity formation [28]. Since then, monastrol and its derivatives have been used as stimulus and template for the design of new anticancer drugs [29]. Going forwards, to better understand the mechanism of action of novel THPMs the interactions with DNA and BSA were further performed. The interaction between small molecules and DNA or BSA can be useful to understand the toxic

* Corresponding author.
E-mail addresses: nenad.jankovic@kg.ac.rs, njankovic@alumnos.uvigo.es (N. Janković).

https://doi.org/10.1016/j.bioorg.2019.02.026
Received 2 November 2018; Received in revised form 3 January 2019; Accepted 9 February 2019
Available online 12 February 2019

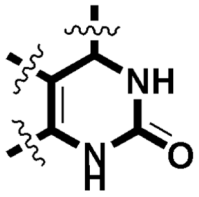

Fig. 1. Structure of 2-oxo-1,2,3,4-tetrahydropyrimidine scaffold.

properties and mechanism of harmful chemicals and for creating new anticarcinogens [30]. Drugs and small bioactive molecules bind reversibly to albumin that is of crucial importance in the transportation and deposition of many bioactive compounds [31].

In addition, matrix metalloproteinase 2 (MMP2) and matrix metalloproteinase 9 (MMP9) have an important role in cervical cancer invasion and metastasis [32]. Matrix metalloproteinase inhibitor 3 (TIMP3) acts as tumor suppressor and induces apoptosis in moderately invasive HeLa cells [33]. miR-21 is a well-known oncomiRNA, overexpressed in a wide range of malignancies [34] and cervical cancer [35], as well. miR-21 has the potential to silence *TIMP3* translation [36], while TIMP3 has the ability to deactivate MMP2 and MMP9. Increased levels of *MMP2*, *MMP9*, miR-21, and decreased levels of *TIMP3* mRNA might be associated with cervical cancer formation and progression, and especially invasive potential of the tumor, because of its involvement in epithelial mesenchymal transition. In cervical cancer, it has been found that higher miR-21 levels were associated with higher levels of the signal transducer and activator of transcription 3 (STAT3) signaling pathway components such as MMP2 and MMP9 [34]. miR-21 overexpression is inversely correlated with inhibitor of matrixmetalloprotienases, TIMP3. miR-21, MMP2, MMP9, and TIMP3 are essential components of STAT3 signaling pathway in the terms of maintaining higher levels of STAT3, especially in human papilloma virus (HPV)-associated cervical cancer formation and progression [34]. It has been shown that miRNA-21 directly targets TIMP3, and thus releases MMP2 and MMP9 secretion in extracellular matrix, which enables the process of angiogenesis [35], and invasion [34]. miR-21 is one of the most prominent oncomiRNAs, in cancer in general [36], and in cervical cancer, as well [34]. Great number of studies investigates various therapeutic strategies that have the goal to inhibit its overexpression, which is the reason why we wanted to see potential effects of our compounds.

Taking into account the importance of Biginelli's products and our previous interest in Biginelli reaction [37–40] twelve novel compounds were synthesized (Fig. 2), characterized and exposed to pharmacological evaluation.

2. Results and discussion

2.1. Chemistry

In this paper, a simple and convenient method for the multicomponent one-pot Biginelli reaction for the synthesis of THPMs derivatives **4a**, **4d-l** and 1,3,5-oxadiazocine **4b** and **4c** from *N*-methylurea (**1**), 4-chloro ethylacetoacetate (**2**) and some aldehydes **3a-l** under different reaction conditions is presented (methods A and B, Fig. 2).

After simple work-up (see Experimental section) the newly-synthesized products **4a-l** were obtained. All the products were characterized by m.p., IR, ^{1}H-, ^{13}C NMR and ESI-MS spectra (see Supplementary Information-SI). The obtained yields and structures of the products **4a-l** are depicted in Fig. 2. Generally, very good to excellent yields were achieved in all cases, but, the best yield (91%) was achieved in the synthesis of **4c**. Interestingly, for synthesis of 1,3,5-oxadiazocine **4b** and **4c** the use of ultrasound irradiation under solvent-free conditions (method B) was necessary to achieve better yields. Compounds **4b** and **4h** were suitable for X-ray crystallographic analyses that are presented in the next section.

2.1.1. Crystallography

Compounds **4b** and **4h** were obtained as single crystals suitable for X-ray diffraction studies. Both compounds crystallized in the same centrosymmetric space group $P2_1/c$ and their molecular structures are shown in Figs. 3 and 4. The most important structural fragment which is common for both molecules is the N1−C1−N2−C2−C3−C4 six-membered heterocyclic ring. This ring has the same composition and equal or similar substituents in both compounds. However two atoms within the ring, the C3 and C4, have different character; they are sp^3 hybridized in **4b** while in **4h** the same atoms are sp^2 hybridized with clear trigonal and coplanar geometry of bonds around them. As a consequence compound **4b** has three optically active centers mutually bonded in the C3−C3−C4 fragment. Two fused six-membered rings only exist in the **4b** molecule and the common structural part for these two rings is above mentioned the C3−C3−C4 fragment. Four atoms from the N1−C1−N2−C2−C3−C4 ring are nearly coplanar in both molecules as one can conclude from the values of the C4−N1−C1−N2 torsion angle that is 2.5(2) and 5.9(5)° in **4b** and **4h** respectively.

There are five N−C bonds but in both compounds the C1−N1 and C1−N2 bonds from ureido fragment are the shortest and mutually very similar (Table S1, SI). Trigonal and coplanar arrangement of the N1−C bonds undoubtedly approves an sp^2 character of the N1 nitrogen atom. The N2 atom bind only one H atom as it is clearly found in the difference electron density maps of both crystal structures. Although two molecules exhibit significant conformational differences and dissimilarity in composition (Figs. 3 and 4), both of them form compact centrosymmetric dimers with molecules interconnected via two rather strong N2−H···O1 bonds. This hydrogen bond in both molecules has the N2−H···O1 angle close to 180° and the N2···O1 interatomic distance below 3.0 Å. Geometry of the dimers in two compounds is very similar as it is illustrated in Fig. S25 (SI).

2.2. Biological evaluation

2.2.1. Cytotoxic activity

The newly synthesized compounds (**4a-l**) were evaluated for *in vitro* cytotoxic activity against three human tumor cell lines, cervix adenocarcinoma cell line (HeLa), human colon carcinoma (LS174), non-small cell lung carcinoma (A549) and a on normal cell line, human fetal lung fibroblast cell line (MRC-5) by employing a MTT assay (Table 1).

Based on the obtained IC_{50} values in Table 1, it was observed that compounds **4c**, **4d**, **4f**, **4k** and **4l** showed strong activity against all tested malignant cell lines, similar to the activity of cisplatin which is used as a reference compound. Compounds **4g** and **4h** also showed good activity, while **4i** exhibited somewhat weaker to moderate cytotoxic activity against tested malignant cell lines. Compound **4b** showed the weakest activity against all tested malignant cell lines.

IC_{50} values for **4c-l** are ranging from 6.03 ± 0.41 to 36.53 ± 0.17 μM indicate that all compounds exhibited significant *in vitro* cytotoxic activity against the all tested tumor cell lines compared with **4a** and **4b**, suggesting that the presence of substituents on aromatic ring in Ar-fragment (Fig. 2) contributes its improved cytotoxicity. Compared with other, **4l** posses the lowest IC_{50} values, demonstrating that the presence of a bromine atom is probably related to its better cytotoxic activity.

From the obtained data, we can see that the investigated compounds exhibit significant differences in cytotoxic activity according to normal MRC-5 cells. Namely, the compounds **4f-i** exhibit low cytotoxicity according to the MRC-5 and consequently very good selectivity. From the above data, we can conclude that **4c-e** and **4j-l** posses better activity compared with *cis*platin on A549 cancer cell lines. Also, it is very important to notice that **4f-i** have up to three times higher selectivity than *cis*platin. Based on previous, the compounds **4c**, **4d**, **4f**, **4k** and **4l** were selected for further evaluation.

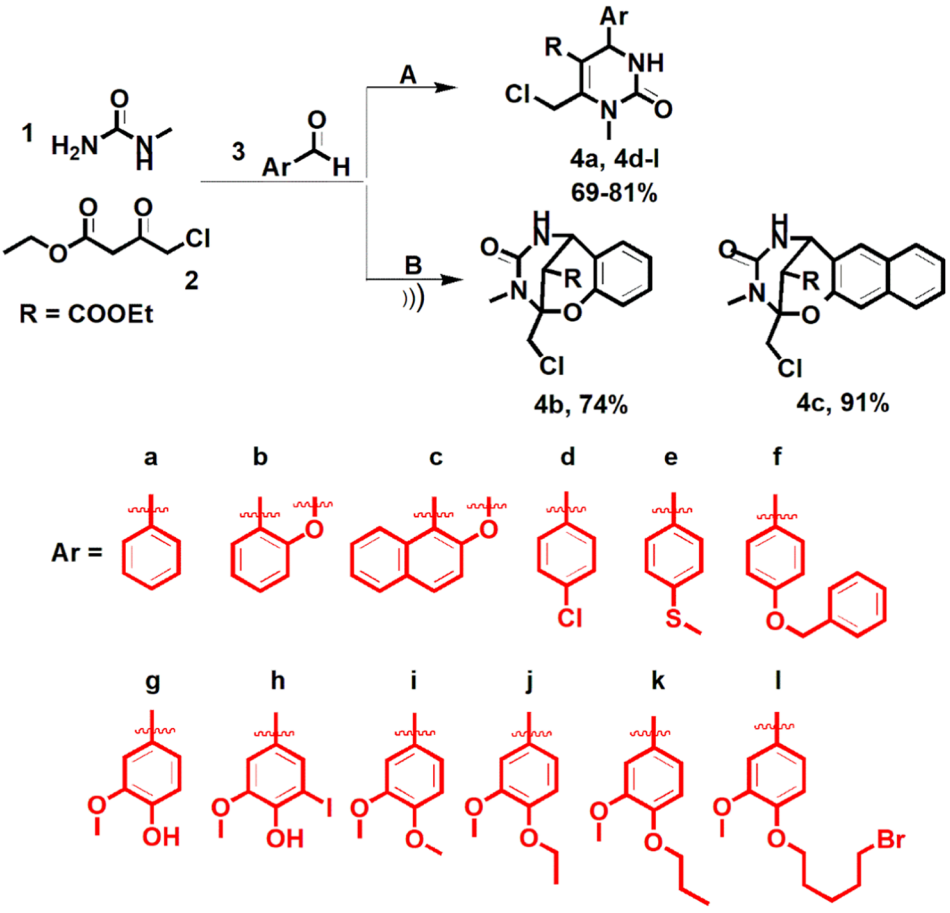

Fig. 2. General outline for the synthesis of the 2-oxo-1,2,3,4-tetrahydropyrimidines **4a**, **4d-l** (A = HCl, ethanol, reflux) and 1,3,5-oxadiazocine **4b** and **4c** (B = HCl, 80 °C).

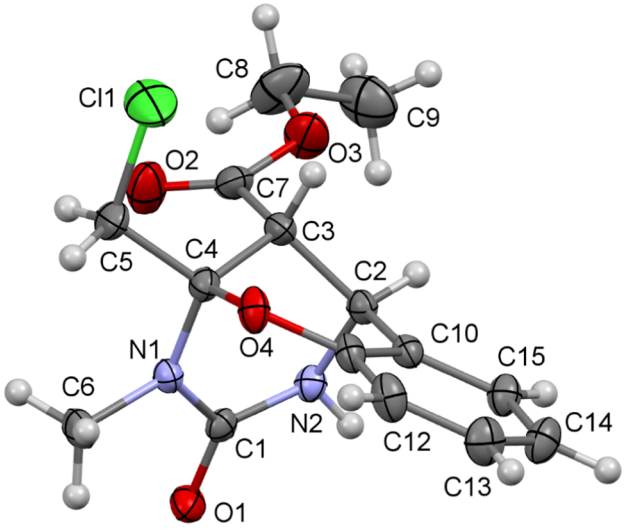

Fig. 3. Molecular structure and numbering scheme of **4b** shown with atomic displacement parameters at the 30% probability level.

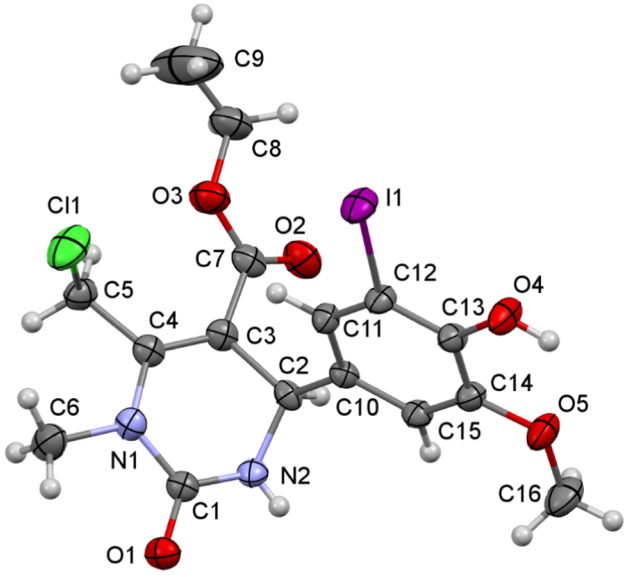

Fig. 4. Molecular structure and numbering scheme of **4h** shown with atomic displacement parameters at the 30% probability level.

2.2.2. Cell cycle distribution

Cell cycle and apoptosis play essential roles in the regulatory mechanisms of cell growth. Suppression of cancer cell growth by many anticancer agents correlates with arrest the cell cycle at the G0/G1, S, and G2/M phase and then induce apoptosis. Hence, the effect of selected compounds **4c**, **4d**, **4f**, **4k** and **4l** on the cell cycle was investigated, to elucidate the mechanisms underlying to their cytotoxic activity. Fig. 5 shows a cell-cycle distribution of HeLa cells incubated in the absence or presence of compounds (IC_{50}) for 24 h, the approximate doubling time of this cell line. Flow cytometry analysis demonstrated that treatment of HeLa cells with **4c**, **4d**, **4k** and **4l** significantly increased the proportion of cells in the sub-G1 phase. A significant

Table 1
Concentrations of compounds that induced a 50% decrease in HeLa, LS174, A549 and MRC5 cell survival rate [expressed as IC_{50} (μM)]. The compounds were incubated with cells for 72 h.

Compounds	IC_{50} (μM)			
	HeLa	LS174	A549	MRC5
4a	42.30 ± 0.74	37.52 ± 1.80	32.66 ± 0.51	191.22 ± 1.72
4b	147.18 ± 2.53	128.31 ± 3.46	85.92 ± 1.28	> 200
4c	9.43 ± 0.73	6.51 ± 1.31	7.27 ± 1.52	3.80 ± 0.92
4d	7.63 ± 0.03	6.49 ± 1.04	7.49 ± 2.46	2.71 ± 0.17
4e	10.64 ± 0.52	7.49 ± 0.55	8.31 ± 0.02	4.37 ± 0.64
4f	8.12 ± 0.39	10.96 ± 1.24	13.21 ± 0.81	147.55 ± 3.42
4g	9.59 ± 0.72	11.27 ± 0.92	18.11 ± 0.66	122.53 ± 2.65
4h	11.05 ± 0.74	15.48 ± 0.72	18.59 ± 2.43	168.39 ± 4.08
4i	16.61 ± 1.88	24.53 ± 1.45	36.53 ± 0.17	131.77 ± 3.19
4j	9.60 ± 1.16	7.04 ± 0.60	8.99 ± 1.24	4.95 ± 0.60
4k	8.67 ± 0.03	6.91 ± 0.15	7.42 ± 0.56	4.68 ± 0.45
4l	6.03 ± 0.41	8.15 ± 0.56	8.94 ± 0.93	5.59 ± 1.40
Cisplatin	2.37 ± 0.28	4.83 ± 0.35	11.59 ± 1.64	14.32 ± 1.28

IC_{50} values are expressed as the mean ± SD determined from the results of the MTT assay in two independent experiments.

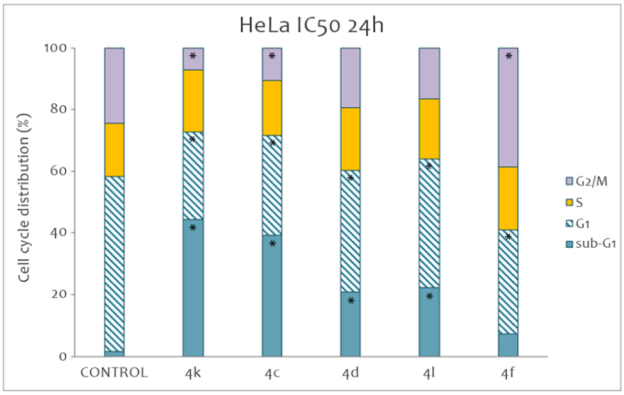

Fig. 5. Cell cycle analysis of HeLa cells untreated (control) and treated with the IC_{50} concentration of compounds **4c**, **4d**, **4f**, **4k** and **4l** for 24 h. Cell-cycle distribution was measured by flow cytometric analysis of DNA content after treatment with these compounds. The results are presented as the mean ± SD of three independent experiments. Statistically significant differences between control and treated cell samples are marked with * ($p < 0.05$).

increase in the sub-G1 phase followed by a G1 phase arrest is accompanied by a concomitant proportional decrease in the percentage of cells in the G2/M phase. The percentage of cells in the G2/M phase was decreased with concentration of IC_{50} and the results were statistically significant ($p < 0.05$) compared with control.

Interestingly, as shown in Fig. 5, the compound **4f** caused a statistically significant increase in the accumulation of cells in the G2/M phase and significantly less changes in the sub-G1 phase than the control ($p < 0.05$). The G2/M arrest is associated with reduction in G1 phase. The obtained results indicate that investigated compounds are inducing apoptosis. Apoptosis maintains the balance between cell proliferation and cell death, and all compounds that promote apoptosis have anti-cancer potential [41]. Our obtained data indicate that compounds-mediated accumulation of sub-G1-G1 phase would most likely be caused by inactivation of Cdk4/cyclin D1 kinase complex. This mechanism has already been confirmed by many data, and it is well known that cyclin D1 and CDKs are essential for driving cells to pass the restriction point [42,43]. Also, the results showed that **4f**, leads to a significant G2/M arrest. As we know, cyclin B-Cdc2 plays a major role in the G2/M phase transition [44,45].

2.2.3. Caspase activities

The activities of caspase-3, -8 and -9, in **4c**, **4d**, **4f**, **4k** and **4l**, treated HeLa cells were detected by specific caspase inhibitors using flow cytometry. As shown on Fig. 6, the exposure of HeLa cells by tested compounds significantly increased the subdiploid DNA content of the HeLa cells, when compared with the control. However, it is evident that the cells were pretreated with caspase-3 and -8 inhibitors and then treated with compounds, did not show significantly reduced levels of subdiploid DNA content. In contrast, the obtained data show that there is a significant reduction in the DNA content of Hela cells pre-treated with caspase-9 inhibitors and compounds **4c** and **4k**, while for **4d**, **4f** and **4l**, this reduction is lower (Fig. 6). In accordance with these results, we can conclude, investigated compounds promoted caspase-9 activation, implicated in the intrinsic pathway of apoptosis [46,47].

2.2.4. Inhibition of tube formation of EA.hy926 cells

Angiogenesis is the process in which new vessels emerge from existing endothelial lined vessels. Angiogenesis is a prerequisite for tumor growth and metastasis formation. Therefore, compounds with anti-angiogenic potential are of importance for cancer treatment [48].

As can be seen on Fig. 7, the EA-hy926 cells after 24 h culture on Matrigel had become organized into three-dimensional capillary-like tubes. EA.hy926 cells treated with subtoxic IC_{20} concentrations of **4f** forming fewer tubes as well as lesser and weaker junctions.

Also, it is evident that **4c**, **4d**, **4k** and **4l** significantly inhibited the angiogenesis of endothelial cells; namely, IC_{20} concentrations induced a nearly complete disruption of the capillary (see Fig. 7).

2.2.5. Gene and microRNA expression levels

miR-21 is a well-known oncomiR, an indicator of invasive potential, involved in epithelial mesenchymal transition. All of our treated samples showed slightly higher levels of miR-21 compared with non-treated cells (Fig. 8). Compound **4k** had the highest miR-21 levels of expression, while **4l** had the lowest. Interestingly, samples treated with **4k** showed lowest levels of MMP2 and MMP9, and higher levels of TIMP3, compared with control, non-treated sample, which might be the compound with the ability to sequester anti-invasive ability, i.e. might inhibit cancer progression. Compound **4d** showed the highest levels of MMP2 and MMP9 and the lowest level of TIMP3, which shows that this compound has the lowest ability to prevent cancer progression (Fig. 8).

The fact that all treated samples showed slightly higher miR-21 levels than the control may not describe the potential influence of the compounds, but it describes varieties in the invasive potential and ability of examined compounds. Those examined compounds might have an anticancer effect in terms of lowering levels of MMP2 and MMP9 and increasing levels of anti-invasive TIMP3 mRNA, but miR-21 was slightly upregulated in the sample treated with the **4k**. MicroRNAs might silence large number of different target genes simultaneously, so it might also be important to silence oncomiRs, such as miR-21 at the

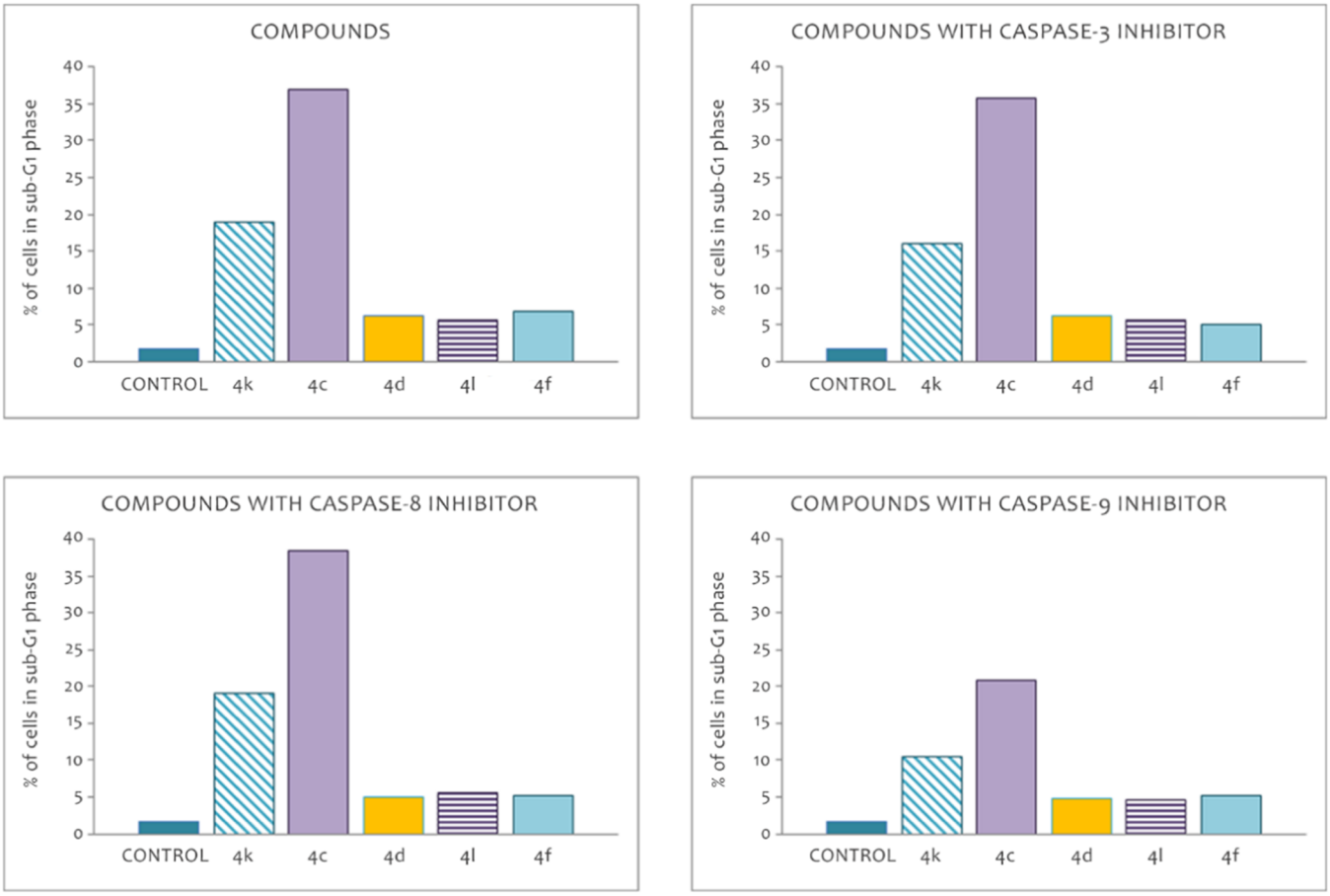

Fig. 6. Effects of caspase inhibitors (caspase-3, -8 and -9 inhibitor) on the percentage of apoptotic HeLa cells after 24 h treatment with compounds. HeLa cells were exposed to IC_{50} concentrations of investigated compounds for 24 h in the presence of specific caspase inhibitors (final concentration – 40 μM) as described.

same time. Our results indicate that along with our examined compounds, there should be introduced one of the miRNA inhibition strategies, such as lock nucleic acid (LNA) antimiRNAs, small molecules inhibitors of miRNAs (SMIRs), antagomiRNAs, miRNA zipper, as well [49]. By combining two models (in our case **4k** and anti-miR-21), oncomiRNA can be silenced, as well as genes involved in cancer progression by examined compounds, similarly as in the experiment of Liu et al. [50], which examined combination of anti-miR-122 direct-acting antivirals (DAAs) in HCV-related HCC treatment. In fact, two strategies can achieve a synergistic effect, which was shown by Devulapally et al. [51]. The same authors used a combination of ASO anti-miR-21-PS and 4-OHT, which have shown a synergistic effect on inhibiting proliferative abilities of estrogen receptor positive (ER +) breast cancer cell line models [51].

Cervical cancer, as well as other cancer models is a heterogeneous disease, and conventional therapies have numerous limitations, so it is necessary to introduce novel strategies for its treatment, especially combined treatments, along with conventional therapies [52].

2.3. Viscosity measurements

Viscosity measurements were performed in order to study the influence of ligands **4c** and **4d** on the relative specific viscosity of DNA. The relative specific viscosity (η/η_o) of DNA is firmly dependent on the length changes that may associate with the separation of DNA base pairs caused by intercalative interaction between DNA's double helix and a small molecule. Based on this it is well-known that intercalated ligands cause lengthening of the DNA helix and increases its relative viscosity [53]. The groove binding or electrostatically interacting ligands kinks or bends the DNA helix and reduces its effective length and, consequently, it exerts substantially no effect on DNA viscosity [54]. A classical DNA intercalator leads to a significant increase in the viscosity of the DNA. In our case, relative viscosity increases with a slope value of 0.58 (ligand **4d**) and 0.47 (ligand **4c**). Upon addition of both ligands to DNA, the relative viscosity increases steadily, as in the case of the classical intercalator (Fig. S26). The results suggest that the ligands bind with DNA through the intercalative mode since the viscosity increase of DNA is ascribed to the intercalative binding mode, which causes the effective lengthening of the DNA [55]. Therefore, the viscosity increment in the DNA caused ligands **4c** and **4d** to offer auxiliary support for the intercalative mode of interaction with DNA. To compare binding affinity of investigated compounds the slope of relative viscosity was discussed. The higher values are obtained for ligand **4d** (0.58) indicating more dominant intercalation effect on other interactions.

2.4. Molecular docking study

The molecular docking was performed to support the interactions and to find out the preferred binding modes of ligands (**4c** and **4d**) with DNA, as well as reference compound, cisplatin. The best-docked poses of the compounds with DNA dodecamer are displayed in Fig. 9, and calculated results for binding energies and docked inhibition constant are summarised in Table 2.

Docking analysis shows that both compounds have conformational changes during docking and as a result, only benzene rings interact through intercalation with DNA. As can be seen from schematic representation of an interaction, the **4d** ligand interact with DNA base

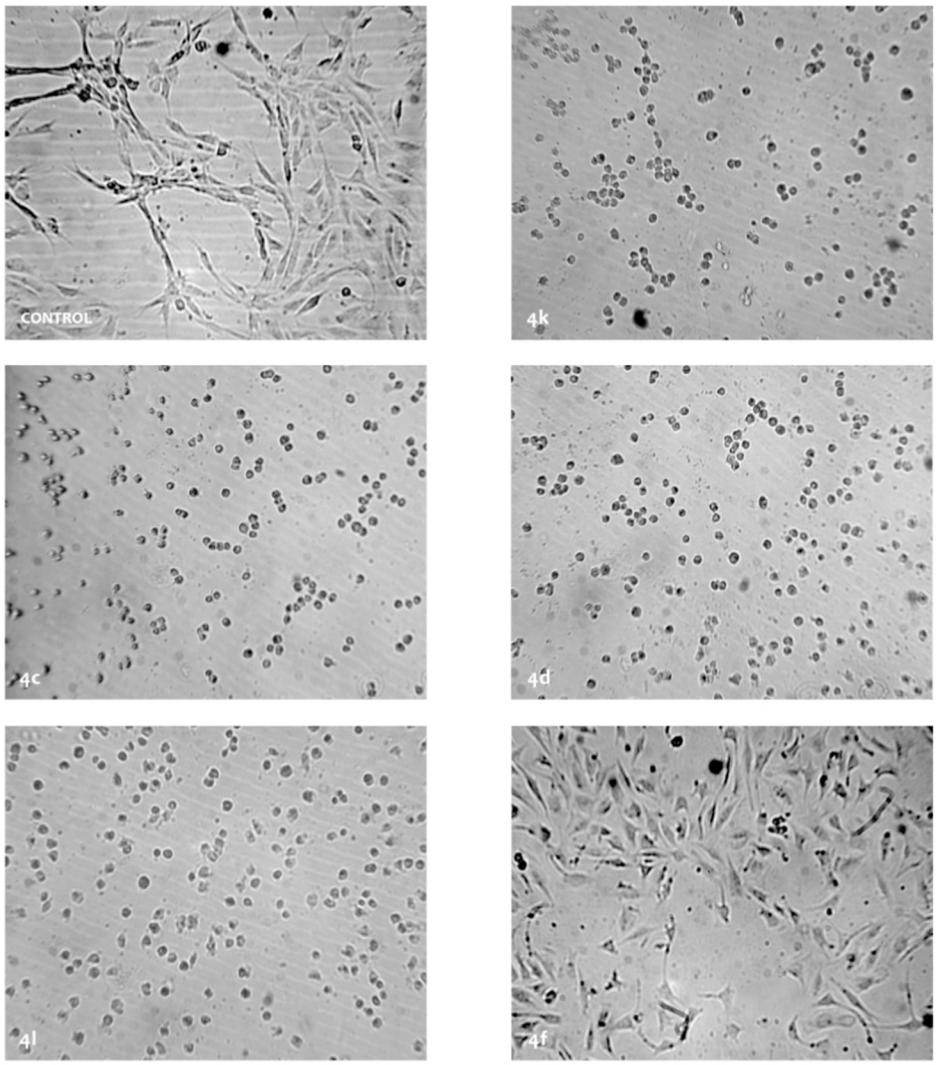

Fig. 7. Effects of compounds **4c**, **4d**, **4f**, **4k** and **4l** on angiogenesis of endothelial EA.hy926 cells. Applied concentrations of compounds are subtoxic (IC_{20}). Representative photomicrographs of one out of two independent experiments are shown.

pairs through van der Waals and hydrophobic interactions, as well as the formation of hydrogen bond between NH and DA:A6 and DT:A7. On the other hand ligand **4c** form only one hydrogen bond with DT:A7. The existence of one more hydrogen bond between DNA molecule and **4d** lead to better binding (lower binding energy values), which is in accordance with results of viscosity measurements, due to lower values of the slope of ligand **4d** comparing to ligand **4c**.

From Table 2, **4d** have a more negative value of free binding energy (ΔG), a priori highest binding affinity towards DNA comparing to **4c**. These results lead to the conclusion that additional formation of H-bonds has less influence on the binding of ligands to DNA molecule comparing to geometrical fitting.

By comparison of results with *cis*platin, published in our previous work [23], similar values for ΔG are obtained for ligand **4d**. Molecular docking analysis of ligands with BSA was performed to validate the experimental results and to determine the possible binding modes and binding sites. The results of docking studies of the compounds with BSA receptor are summarised in Table 2, and the 3D binding environment is presented in Fig. 10. Analysis of results shows that all ligands interact with BSA in the same binding pocket (Fig. 10). The ligand **4d** is forming three H-bonds, with Asp 118, Lys 136 and with Glu-125. The interaction between ligand **4c** and BSA is stabilised due to hydrogen bond formation with Lys 136 and Glu 140. From obtained results, it can be noted that most responsible amino acid residue for binding of investigated compounds with BSA is Lys 136. By analysing of results for ΔG, between ligands **4d** and **4c**, ligand **4d** have lower values, which indicate a stronger binding affinity towards BSA. This observation leads to the conclusion that the smaller size of **4d** allows more comfortable fitting in the structure of BSA, which is manifested by lower binding energy. In comparison with results obtained for cisplatin docking, ΔG values for cisplatin were significantly lower.

2.5. Lipophilicity assessment and structure active relationship

2.5.1. Multivariate statistical analysis

Different molecular descriptors (constitutional, geometric and topological) were calculated for each compound and presented in Table S3 (SI). Molecular descriptor values as well as experimentally obtained lipophilicity data (Table S4, $\log k_w$) were employed in hierarchical cluster analysis (HCA) and principal components analysis (PCA).

In this work, HCA is used to build a hierarchical tree considering similar attributes between compounds. Euclidean distance, group average cluster method and sum of distances were applied in clustering of molecules. Distance generated by variables varies between 0 and 1, where 1 represents maximal distance. According to the dendrogram, twelve molecules were grouped in two major clusters (Fig. 11). Only two compounds (**4f** and **4l**) belong to the second cluster, and they possess higher lipophilicity values. First cluster groups more

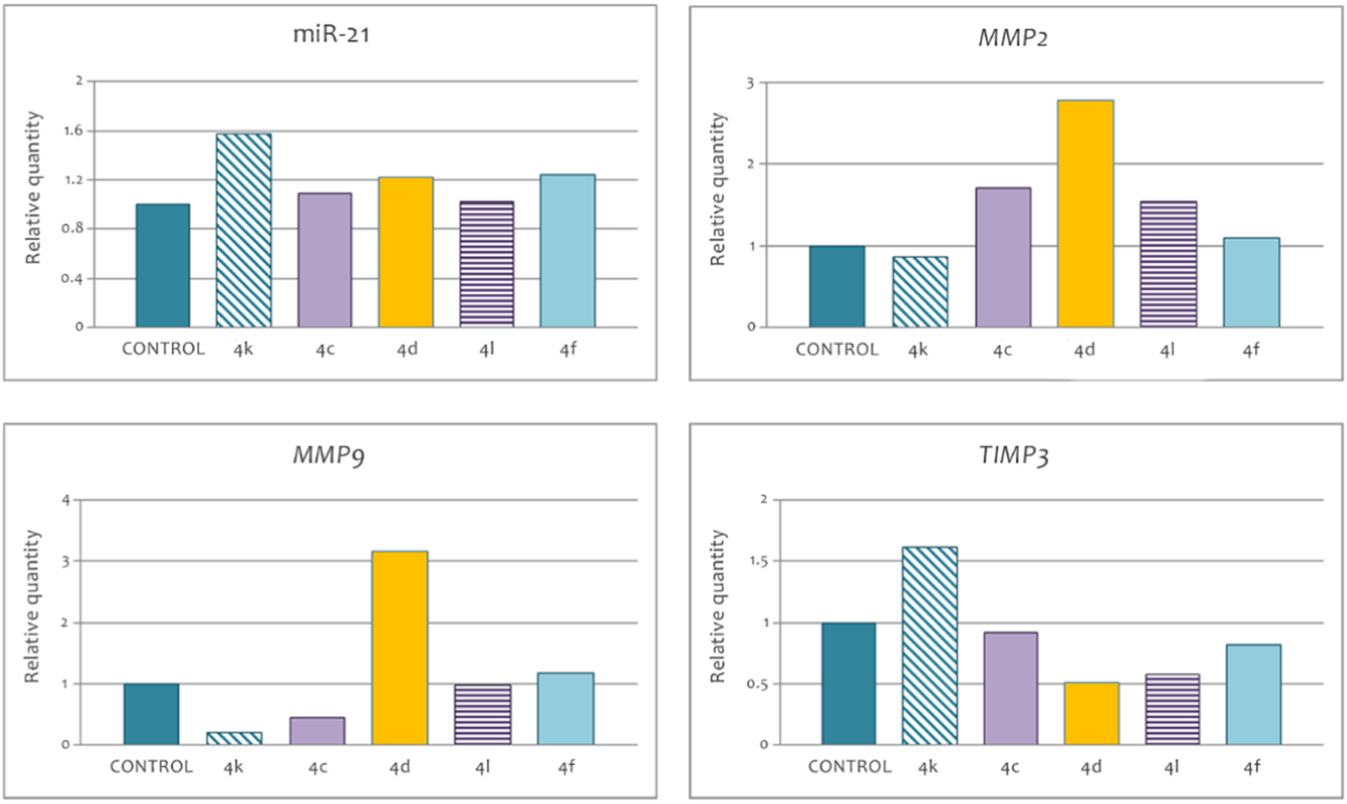

Fig. 8. Changes in expression levels of miR-21, MMP2 gene, MMP9 gene, and TIMP3 gene in HeLa cells exposed to subtoxic IC_{20} concentrations of the compounds **4c**, **4d**, **4f**, **4k** and **4l** for 24 h.

hydrophilic molecules where compounds **4c**, **4d** and **4k** show best biological activity. Compounds **4c**, **4d**, **4e** and **4k** contain a heteroatom as the substituent which probably influences stronger cytotoxicity. In the second cluster both molecules **4l** and **4f** show significant cytotoxic activity and probably the presence of the benzyl group and the bromine could explain the stronger biological activity. Only the most hydrophobic compounds were grouped in the second cluster due to their bulky highly lipophilic substituents.

The purpose of PCA is not only to reduce descriptors' number but also to correlate descriptors in order to find other variables and to group selected descriptors in principal components. PCA was applied in our data set in order to gain an overview of similarity or dissimilarity among the examined molecules. Regarding our data set, first two principal components have explained 94.18% of the total variance from original data, thereby PC1 described 71.84%. In the Fig. 11, (table D) are presented selected descriptors which most influenced the similarities/dissimilarities between compounds. In PC1 descriptor values (Mw, W, V, TPSA and log k_w) are ranged from 0.52 to 0.2. For PC2 descriptor TPSA showed the highest loading values. Regarding the biplot Fig. 11(C) it can be concluded that HCA and PCA gained similar findings. Heatmap with IC_{50} activity values of all examined molecules (n = 12) is provided in Fig. 12 in order to better visualize activity data. Compounds with the highest lipophilicity values (**4c**, **4d**, **4f**, **4k**, and **4l**) exhibit stronger anticancer potential.

2.5.2. The Molecular Lipophilicity Potential (MLP) and Polar Surface Area (PSA)

The molecular characteristics highlighted as valuable for biologic activity in HCA and PCA analysis (Fig. 11) and information from the compounds' activity regarding the nature of substituents (Fig. 12) were considered as appropriate for selection of two descriptors (TPSA and experimentally obtained values of lipophilicity; log k_w) to be further examined. Logk_w and Topological surface area (TPSA) values can be visualized in Fig. 13 comparing the most active compounds: **4c**, **4d**, **4e**, **4k** and **4l**.

Lipophilicity represents the molecular property which is widely investigated in SAR and QSAR approaches. This characteristic can affect biological activity of the molecule such as permeation of a molecule through biological tissues/barriers, as well as interactions with transporter proteins and enzymes [56].

MLP is particularly helpful in explanation of different ADME properties of compounds. Analysis of the 3D distribution of hydrophobicity on the molecular surface can be useful in explanation of differences between observed ADME characteristics with same log*P*. The biological activity of the investigated compounds has not been strictly related to lipophilicity. Compound **4l** shows the highest cytotoxic activity and higher values of log k_w compared to the other most promised candidates: **4c**, **4d**, **4f** and **4k**. These molecules show moderate values of lipophilicity as well as moderate values of TPSA.

3. Conclusion

A simple and convenient method for the multicomponent one-pot Biginelli reaction for the synthesis of THPMs derivatives **4a-l** from *N*-methylurea (**1**), of ethyl 4-chloroacetoacetate (**2**) and some aldehydes **3a-l** under different reaction conditions is presented. Synthesized compounds (**4a-l**) were evaluated for *in vitro* cytotoxic activity against cervix adenocarcinoma cell line (HeLa), human colon carcinoma (LS174), non-small cell lung carcinoma (A549) and an on the normal cell line, human fetal lung fibroblast cell line (MRC-5) by employing a MTT assay. Compounds **4c**, **4d**, **4f**, **4k** and **4l** showed strong activity against all tested malignant cell lines, similar to the activity of cisplatin. Also, the compounds **4f-i** exhibit low cytotoxicity according to the MRC-5 and consequently very good selectivity. The molecular docking was also performed to support the interactions and to find out the preferred binding modes of ligands (**4c** and **4d**) with DNA and BSA.

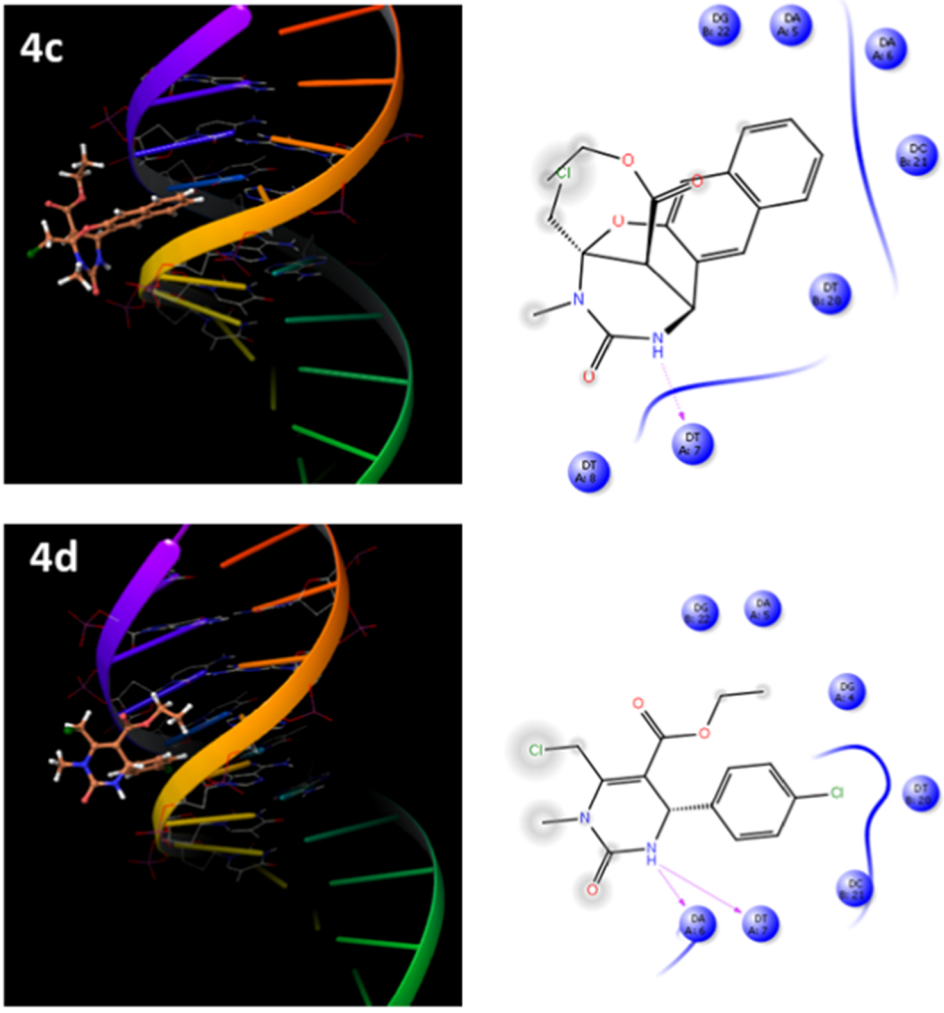

Fig. 9. Visual representation of binding environment for ligands **4c** and **4d** with DNA along with a schematic representation of interactions.

Table 2
Results of docking score, free energy of binding and docked inhibition constant for investigated ligands.

Ligand	Docking score	Free energy of binding (ΔG)/kJ mol^{-1}	Docked inhibition constant (K_i)/μM
	DNA		
4c	−4.252	−32.82	1.775
4d	−4.884	−38.78	0.160
Cisplatin	−6.345	−37.06	0.304
	BSA		
4c	−5.002	−43.55	0.024
4d	−4.169	−44.76	0.014
Cisplatin	−5.321	−20.18	291.35

Obtained results show that for both compounds only benzene rings interact through intercalation with DNA. Analysis of results for BSA shows that all ligands interact with BSA in the same binding pocket. Results of Multivariate Statistical Analysis indicated that compounds **4c**, **4d**, **4e** and **4k** shows moderate lipophilicity and contain a heteroatom as the substituent which probably influences stronger cytotoxicity. Compounds with heteroatom and/or alkyl group at position 4 of the benzene ring (**4k**, **4j**, **4l**, **4d**, **4e** and **4c**) exhibit stronger anticancer potential.

4. Experimental

4.1. Chemistry

All solvents and substrate were purchased from Sigma. The alkylation of aldehydes was done according to the previously described methodology [57]. Melting-points (Mp) were determined on a Mel-Temp apparatus and are uncorrected. Thin-layer chromatography (TLC) was carried out on 0.25 mm Sigma-Aldrich coated silica gel plates (60F-254) using eluent DCM:EtOAc (9:1) mixture as a mobile phase and UV light for visualization. The IR spectra were recorded by a Perkin–Elmer Spectrum One FT-IR spectrometer on KBr pellet. The NMR spectra of compounds Ethyl 6-chloromethyl-1-methyl-2-oxo-4-phenyl-1,2,3,4-tetrahydropyrimidine-5-carboxylate (**4a**), 2,6-Methano-2H-1,3,5-benzoxadiazocine-11-carboxylic acid, 4,5,6-trihydro-2-chloromethyl-3-methyl-4-oxo-, ethyl ester (**4b**), 1,5-Methano-1H-naphth[1,2–g][1,3,5] oxadiazocine-13-carboxylic acid, 2,3,4,5-tetrahydro-5-chloromethyl-4-methyl-3-oxo-, ethyl ester (**4c**), Ethyl 6-chloromethyl-1-methyl-2-oxo-4-(4′-chlorophenyl)-1,2,3,4-tetrahydropyrimidine-5-carboxylate (**4d**), Ethyl 6-chloromethyl-1-methyl-2-oxo-4-(4′-methylthiophenyl)-1,2,3,4-tetrahydropyrimidine-5-carboxylate (**4e**), Ethyl 6- (chloromethyl)-1-methyl-2-oxo-4-(4′-benzyloxyphenyl)-1,2,3,4-tetrahydropyrimidine-5-carboxylate (**4f**), Ethyl 6-chloromethyl-1-methyl-2-oxo-4-(4′-hydroxy-3′-methoxyphenyl)-1,2,3,4-tetrahydropyrimidine-5-carboxylate (**4g**), Ethyl 6-chloromethyl-1-methyl-2-oxo-4-(4′-hydroxy-5′-iodo-3′-methoxyphenyl)-1,2,3,4-tetrahydropyrimidine-5-carboxylate (**4h**), Ethyl 6-

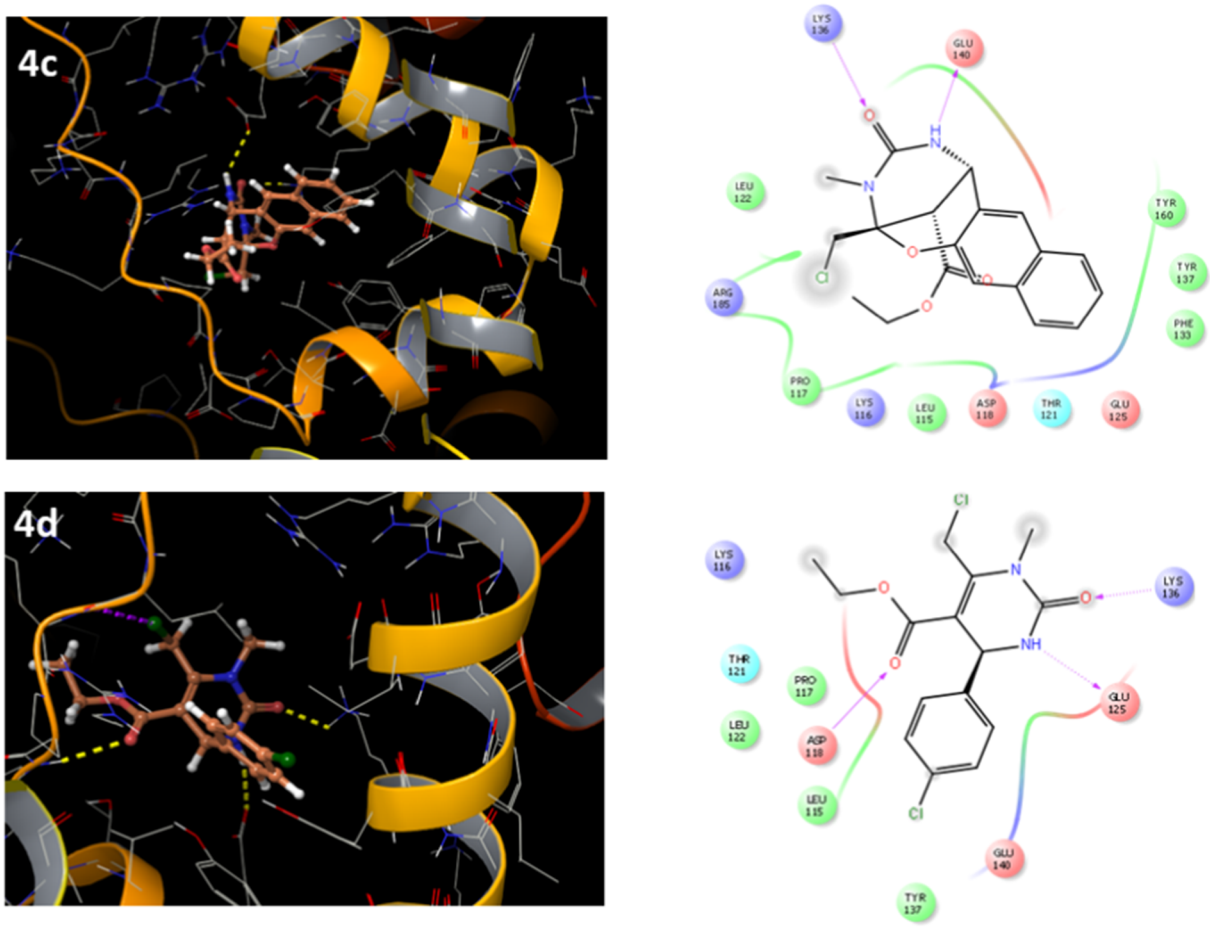

Fig. 10. Representation of binding environment for ligands **4c** and **4d** with BSA along with a schematic representation of interactions.

chloromethyl-1-methyl-2-oxo-4-(3′,4′-dimethoxyphenyl)-1,2,3,4-tetrahydropyrimidine-5-carboxylate (**4i**), Ethyl 6-chloromethyl-1-methyl-2-oxo-4-(4′-ethoxy-3′-methoxyphenyl)-1,2,3,4-tetrahydropyrimidine-5-carboxylate (**4j**), Ethyl 6-chloromethyl-1-methyl-2-oxo-4-(3′-methoxy-4′-propoxyphenyl)-1,2,3,4-tetrahydropyrimidine-5-carboxylate (**4k**), and Ethyl 6-chloromethyl-1-methyl-2-oxo-4-(4′-bromo-*n*-pentyloxy-3′-methoxyphenyl)-1,2,3,4-tetrahydropyrimidine-5-carboxylate (**4l**) were performed in $CDCl_3$ or DMSO-d_6, with TMS as internal standard on a Varian Gemini 200 MHz NMR spectrometer (^{1}H at 200 and ^{13}C at 50 MHz). Abbreviations for the NMR signal that were used are: s = singlet, d = doublet, t = triplet, m = multiplet, and dd = doublet of doublet. All NMR (^{1}H and ^{13}C) spectral data given in SI (see Figs. S1–S24). Mass spectrometry was performed by Waters Micromass Quattro II triple quadrupole mass spectrometer and MassLynx software for control and data processing. Electrospray ionization in the positive mode was used. The electro spray capillary was set at 3.0 kV and the cone at 20 V. The ion source temperature was set at 120 °C and the flow rates for nitrogen bath and spray were 500 l/h and 50 l/h, respectively. The collision energy was 20 eV.

4.1.1. General experimental procedures

*4.1.1.1. Synthesis of **4a, 4d-l** (method A).* To 6.5 mmol of *N*-methylurea ethanol solution in a 50-mL round-bottom flask, mixture of ethyl 4-chloroacetoacetate (5 mmol) and aldehyde (5 mmol) dissolved in 15 mL of bubbled ethanol was add and after that 0.1 mL HCl (36.5%) was added dropwise. The reaction was followed by TLC (eluent EtOAc : *n*-hexane). After cooling, the formed yellow powder was filtered, washed with DCM, cold ethanol and water and recrystallized from boiling methanol to achieve the desired product with a good purity grade.

*4.1.1.2. Synthesis of **4b** and **4c** (method B).* *N*-methylurea (3 mmol), ethyl 4-chloroacetoacetate (3 mmol), aldehyde **1b** or **1c** with five drop of HCl (36.5%) were heated at 80 °C in round bottom flask (50 mL) through 2 h. Upon completion of the reaction in formed solid mixture, 20 mL of hot ethanol was added. After cooling in refrigerator, white crystals of targeted products very fast fallout from solution. Crystals were isolated via filtration, washed with small portions of cold ethanol and dried at room temperature to afford the desired products.

4.2. X-ray data collection and structure refinement for compounds **4b** and **4h**

Single-crystal X-ray diffraction data for both compounds were collected on an Oxford Gemini S diffractometer equipped with a CCD detector, using monochromated Mo Kα radiation. Data reduction and empirical absorption correction were performed with CrysAlisPRO [58]. Crystal structures were solved by direct methods using SHELXS and refined on F2 by full-matrix least-squares using SHELXL [59]. All non-H atoms were refined anisotropically. Positions of H atoms bonded to the N2 nitrogen atoms as well as H atom bonded to the O4 were taken from difference electron density maps. All remaining H atoms were placed in geometrically calculated positions and refined using the riding model with Uiso values constrained to 1.2Ueq or 1.5Ueq of the parent C atoms. Crystallographic details for structure analysis of the compounds **4b** and **4h** are summarized in Table S2. Figures were produced using MERCURY [60]. The software used for the preparation of the materials for publication: WINGX [61], PLATON [62], and PARST [63].

A: HCA of samples

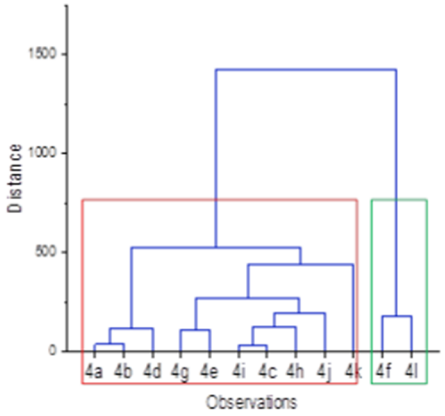

B: Eigenvalues of the correlation

	Eigenvalue	Percentage of Variance	Cumulative
1	3,5918	71.84%	71.84%
2	1,11724	22.34%	94.18%
3	0,24227	4.85%	99.03%
4	0,03375	0.67%	99.70%
5	0,01494	0.30%	100.00%

C: Biplot

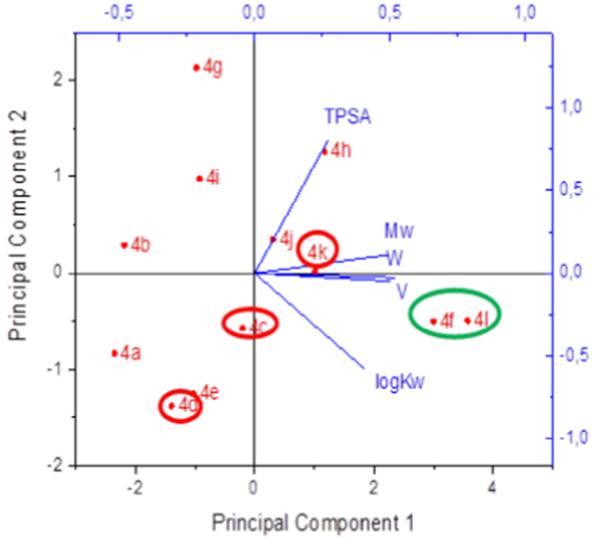

D: Extracted eigenvectors

	Coefficients of PC1	Coefficients of PC2
Mw	0,49283	0,11255
V	0,51838	-0,02787
W	0,50065	-0,05035
LogKw	0,40505	-0,57891
TPSA	0,27146	0,80553

Fig. 11. HCA analysis: (A) Dendrogram of investigated compounds with two main clusters: red marked (more hydrophilic compounds with less bulky substituents) and green marked (lipophilic compounds with bulky substituents). PCA analysis: (B) Eigenvalues of the correlation matrix: the two first factors PC1 and PC2 explained 94.27% of total variance from the original data; (C) Biplot for the two first factors PC1 versus PC2 and molecular descriptors; (D) Extracted eigenvectors of PC1 and PC2: coefficients of PC1 and PC2 are presented in columns.

4.3. Biological activity

4.3.1. Cell culture

Cervix adenocarcinoma cell line (HeLa), human colon carcinoma (LS174), non-small cell lung carcinoma (A549) and a normal cell line, human fetal lung fibroblast cell line (MRC-5) were grown in RPMI-1640 medium (Sigma) at 37 °C. Media were supplemented with 10% fetal bovine serum, L-glutamine, and penicillin-streptomycin (Sigma).

4.3.2. Treatment of cells

Stock solutions (10 mM) of the compounds, made in DMSO, were dissolved in a corresponding medium to the required working concentrations. Target cells HeLa (2000 cells per well), LS174 (7000 cells per well), A549 (5000 cells per well) and MRC-5 (5000 cells per well) were seeded into wells of a 96-well flat-bottomed microtitre plate. Twenty-four hours later, after the cell adherence, different concentrations of investigated compounds were added to the wells, except for the control cells to which only nutrient medium was added. Final concentrations reached in treated wells were in the range of 12.5 μM to 200 μM. The final concentration of DMSO solvent never exceeded 0.5%, which was non-toxic to the cells. The positive control was chemotherapy drug cisplatin. All investigated concentrations were set up in triplicate. Nutrient medium with corresponding concentrations of investigated compounds, but without cells, was used as a blank, also in triplicate. The cultures were incubated for 72 h.

4.3.3. Determination of IC_{50} value

The effect of the investigated compounds on survival of the specified cell lines was determined by the microculture tetrazolium test (MTT) according to Mosmann [64] with modification by Ohno and Abe [65]

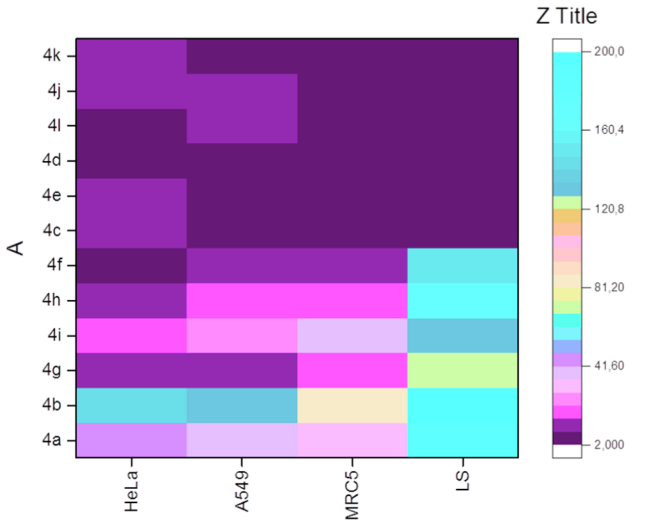

Fig. 12. Cytotoxic activity of **4a-l** examined on HeLa, A549, MRC-5 and LS cell lines. Ranges of IC_{50} values are indicated by the colors: violet-dark blue, 2–41.60 μM; light blue-green, 41.61–81.20 μM; yellow-orange, 81.21–120.8 μM; red, 120.9–160.4 μM; dark red 160.5–200 μM.

72 h after addition of the compounds, as described earlier. Briefly, 20 mL of MTT solution (5 mg/mL phosphate-buffered saline) was added to each well. Samples were incubated for a further **4h** at 37 °C in a humidified atmosphere of 95% air/5% CO_2 (v/v). Then 100 μL of 100 g/L sodium dodecyl sulfate was added to dissolve the insoluble product formazan resulting from conversion of the MTT dye by viable cells. The absorbance (A) at 570 nm was measured 24 h later. The number of viable cells in each well was proportional to the intensity of the absorbance of light, which was read in an enzyme-linked immunosorbent assay (ELISA) plate reader. To determine cell survival (%), the A of a sample with cells were grown in the presence of various concentrations of the investigated compounds was divided by the control optical density (the A of control cells grown only in nutrient medium) and multiplied by 100. In each experiment, the A of the blank was always subtracted from the A of the corresponding sample with target cells. IC_{50} is defined as the concentration of an agent inhibiting cell survival by 50% compared with a vehicle-treated control. All experiments were done in triplicate.

4.3.4. Cell cycle analysis

Cervix adenocarcinoma (HeLa) cells, were seeded in six-well plates (3×10^5 cells/well), and after 24 h treated with investigated compounds, except control cells, and incubated at 37 °C for the next 24 h. Concentrations used corresponded to IC_{50} values. After the incubation, the cells were collected by trypsinization, and fixed in ice-cold 70% ethanol for 1 h on ice, then at −20 °C for at least a week. After fixation, the cells were washed in PBS and pellets obtained by centrifugation were treated with RNase (100 μg/mL) at 37 °C temperature for 30 min and then incubated with propidium iodide (PI) (40 μg/mL) for at least 30 min. DNA content and cell-cycle distribution were analyzed using a Becton Dickinson FACSCalibur flow cytometer. Flow cytometry analysis was performed using a CellQuestR (Becton Dickinson, San Jose, CA, USA) software on a minimum of 10 000 cells per sample [66].

4.3.5. Determination of target caspases

In order to examine the role of caspases involved in the apoptotic cell death induced by the investigated compounds, the percentages of HeLa cells in the subG1 phase pretreated with a caspase-3 inhibitor were determined. HeLa cells were preincubated for 2 h with a Z-DEVD-FMK caspase-3 inhibitor at a final concentration of 40 μM. Caspase inhibitor was purchased from R&D Systems (Minneapolis, USA). The investigated compounds **(4c**, **4d**, **4f**, **4k** and **4l)** were applied to target HeLa cells at concentrations which corresponded to IC_{50} values obtained for 72 h treatment. For each compound, one sample of HeLa cells were not treated with inhibitor and served as a referent sample. After 24 h of incubation, cells were harvested and fixed in 70% ethanol on ice. Samples were stored at −20 °C for one week before PI staining. Changes in the percentages of cells in the subG1 phase were determined by flow cytometry analysis.

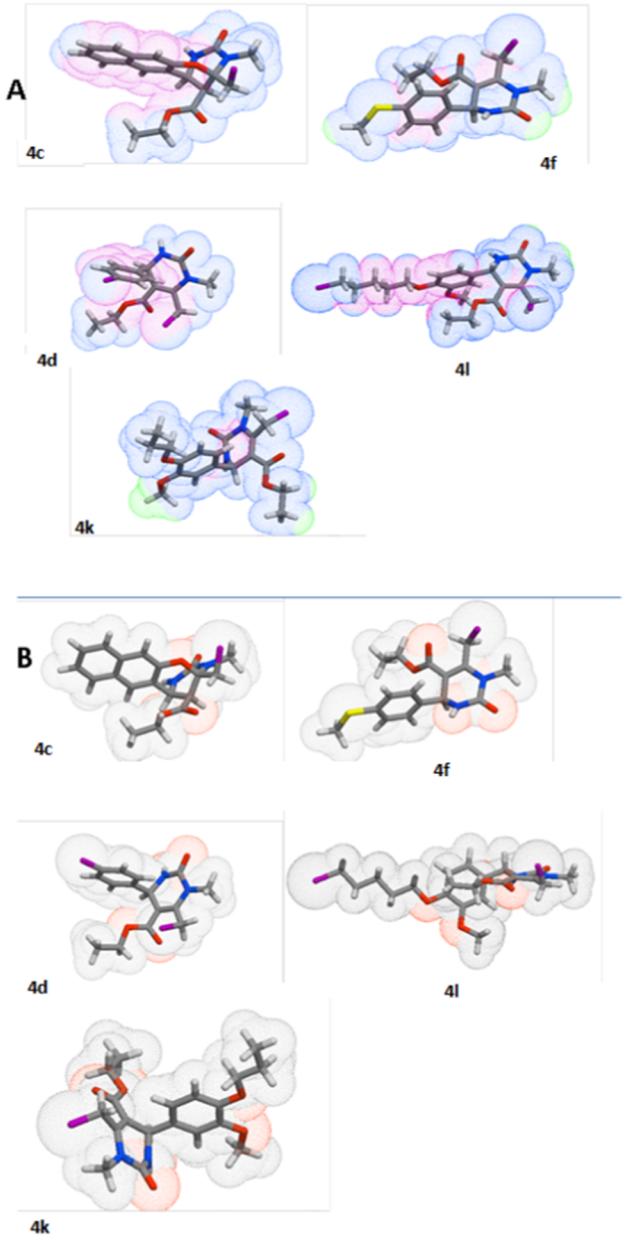

Fig. 13. Presentation of the calculated hydrophobic (miLog*P*) and topological descriptors (TPSA) of the most promising candidates (**4c**, **4d**, **4f**, **4k** and **4l**): (A) map of lipophilic potential (MLP), calculated using the Molinspiration software. MLP is calculated from atomic hydrophobicity contributions, the same method is used in calculation of miLogP values. Galaxy Visualizer provides possibility to visualize molecular lipophilicity potential on the molecular surface to acknowledge hydrophobic (encoded by violet and blue colors) and hydrophilic parts (orange and red) of the molecule. The molecules are shown in the stick model (A and B), where carbon atoms are in gray, oxygen in red, nitrogen in blue, sulphur in yellow, and hydrogen in white. (B) Polar surface area (PSA) was calculate using Molinspiration software. The surfaces are presented by dotted lines. Gray parts correspond to hydrophobic and red to hydrophilic atoms.

4.3.6. Tube formation assay

24-Well plates were coated with 200 µL of Corning® Matrigel® basement membrane matrix (Corning: cat. number 356234). Plates were incubated for 2 h. After that, suspensions of EA.hy926 cells were added into plates. In control cell sample complete nutrient medium was added, while solutions of sub-toxic concentrations (IC_{20}) of compounds with nutrient medium were added to other samples. Those concentrations were obtained by MTT test after 24 h treatment of EA.hy926 cells with investigated extracts. The 24 h incubation in the assay was at 37 °C in an atmosphere of 5% CO_2 and humidified air. After incubation, photomicrographs of target cells were captured under the inverted phase-contrast microscope [67].

4.3.7. Gene and microRNA expression analyses

In this study, we measured changes in the expression levels of MMP2, MMP9, TIMP3, and the levels of miR-21 in human cervical cancer HeLa cells treated with sub-toxic concentrations of five examined compounds. For the extraction of total RNA we used TriReagent (Sigma), isopropanol and 75% diethylpyrocarbonate (DEPC)-ethanol according to manufacturer's protocol. Reverse transcription reaction was performed with High Capacity cDNA Reverse Transcription Kit (Applied Biosystems by Thermo Fisher Scientific, Vilnius, Lithuania) while for real-time quantitative PCR (RT-qPCR) we used No UNG 2x TaqMan Universal Master Mix. Reaction of cDNA amplification was performed with MMP2 (Hs01548727_m1), MMP9 (Hs00957562_m1), and TIMP3 (Hs00165949_m1), and miR-21 (ID 000397) assays. Gene expression, shown in relative quantity (RQ) values, was normalized to GAPDH (Hs02758991_g1), while miR-21 levels were normalized to RNU6B (ID001093) small nuclear RNA. Relative quantity values were obtained by comparative ΔΔCt method, analyzed with 7500 System SDS software (Applied Biosystems, Foster City, California, USA).

4.4. Viscosity measurements

The viscosity of a DNA solution was measured in the presence of increasing amounts of ligands using Ubbelohde viscosimeter (SI Analytics GmbH, Mainz, Germany, type no. 525 03) by measuring the flow rate of the liquid. Viscosimeter was filled with experimental liquid and placed vertically in a glass-sided thermostat maintained constant to ± 0.01 K, with a standard uncertainty of controlled temperature of ± 0.02 K. After thermal equilibrium is attained, the flow time of liquids was recorded with a digital stopwatch with an accuracy of ± 0.001 s. All measurements were performed at 310.15 K. Results were obtained as the mean value of at least ten viscosity measurements, and data were presented as $\left(\frac{\eta}{\eta_o}\right)^{1/3}$ against R, where η is the viscosity of DNA in the presence of ligand, η_o is the viscosity of DNA alone in the buffer solution, and R is mole ratio of ligands/DNA. The DNA concentration was fixed at $1{\cdot}10^{-5}$ mol dm^{-3}. The viscosity values were calculated from the observed flow time of the DNA-containing solutions (t) corrected for the flow time of the buffer alone (t_o), $\eta = \frac{t - t_o}{t_o}$. The relative standard uncertainty of determining the viscosity with Ubbelohde viscosimeter was found to be less than 1%.

4.5. Lipophilicity estimation

Isocratic HPLC measurements were performed using Agilent 1100 Series system with diode array detector. HPLC system possesses binary pump, degasser and automatic injector connected to a computer for information processing with Agilent Chem Station program. As the stationary phase for RP HPLC analysis ZORBAX Eclipse Plus C18 (250 mm × 3 mm, 5 µm) column was used. The organic phase was HPLC grade acetonitrile (Sigma-Aldrich). Flow rate of the mobile phase was 1.00 mL/min. All HPLC measurements were performed following previously published procedure [68]. Retention times for all compounds were determined in duplicate, and the average values were used for determination of log k values (Table S5). The slope (S) and the intercept ($\log k_w$) were calculated by using the Origin Pro 2016 software. The Φ_0 index represents the volume percent of organic phase concentration in the mobile phase by which log k value is 0. The Φ_0 values are calculated from the intercept ($\log k_w$) and the slope (S)

$$\Phi_0 = -\log k_w/S$$

4.6. Molecular modeling and calculation of the descriptor set

For molecular modeling ChemBioDraw Ultra 14.0 and ChemBio3D Ultra 14.0 suit were used in order to create the correct molecular structure (2D and 3D). Adequate 3D chemical structures were undergoing to energy minimization using MM2 force field with a set gradient of 0.1 kcal/Å mol. Geometry optimization was performed using Austin Model 1 and root mean square values for all compounds were lower than 1×10^{-4} kcal/Å mol. Molecular descriptors were calculated using open-source python package ChemoPy [69] and Molinspiration software (http://www.molinspiration.com). Criteria for molecular descriptors selection were: Pearson's linear correlation coefficient between descriptors and IC_{50} values and distribution of data on the scatter plots.

4.7. Computational methods for molecular docking

The structure of the B-DNA dodecamer d(CGCGAATTCGCG)2 (PDB code 1BNA) and bovine serum albumin (BSA) crystal structure (PDB code 3 V03) were used as a model to study the interaction between the investigated ligands and DNA. The structures were processed with the Protein Preparation Wizard in the Schrödinger 2015-02 suite package [70]. The structures integrity was checked and adjusted, and missing residues and loop were added using Prime. Crystallographic water molecules were removed from the DNA fragment. Hydrogen atoms were added after deleting any original ones, followed by adjustment of bond orders for residues and the ligands. The protonation and tautomeric states of residues were adjusted to match a pH of 7. Active site water molecules beyond 5.0 Å from the ligand were deleted. Hydrogen bond sampling with adjustment of active site water molecule orientations was performed using PROPKA at pH 7 [71]. Then, the enzyme was subjected to geometry refinement using an OPLS-2005 force field restrained minimisation with the convergence of heavy atoms to an RMSD of 0.3 Å [72].

The receptor grid for each target was prepared using the OPLS-2005 force field, and docking was performed using Glide with standard precision [73]. Flexible ligand sampling was considered in the docking procedure. All poses were subjected to post-docking minimisation. The lowest binding energy conformer was searched out of 10 different conformers for each docking simulation, and the resultant one was used for further analysis. The best-docked structures for each ligand were determined, based on the model energy score which combines the energy grid score, the binding affinity, the internal strain energy and the Coulomb-van der Waals interaction energy scores.

Conflict of interest

The authors declare no conflict of interest.

Acknowledgements

This work was supported by the Ministry of Education, Science and Technological Development of the Republic of Serbia (Grants 172011 and 41012).

Appendix A. Supplementary material

Supplementary data to this article can be found online at https://doi.org/10.1016/j.bioorg.2019.02.026.

References

[1] A. de Fatima, T.C. Braga, L. Da, S. Neto, B.S. Terra, B.G.F. Oliveira, D.L. da Silva, L.V. Modolo, A mini-review on Biginelli adducts with notable pharmacological properties, J. Adv. Res. (2014), https://doi.org/10.1016/j.jare.2014.10.006.

[2] J. Kim, T. Ok, C. Park, W. So, M. Jo, Y. Kim, M. Seo, D. Lee, S. Jo, Y. Ko, I. Choi, Y. Park, J. Yoon, M.K. Ju, J. Ahn, J. Kim, S.-J. Han, T.-H. Kim, J. Cechetto, J. Nam, M. Liuzzi, P. Sommer, Z. No, A novel 3,4-dihydropyrimidin-2(1H)-one: HIV-1 replication inhibitors with improved metabolic stability, Bioorg. Med. Chem. Lett. 22 (2012) 2522–2526.

[3] R.F.S. Canto, F.A.R. Barbosa, V. Nascimento, A.S. de Oliveira, I.M.C. Brighente, A.L. Braga, Design, synthesis and evaluation of selenodihydropyrimidinones as potential multi-targeted therapeutics for Alzheimer's disease, Org. Biomol. Chem. 12 (2014) 3470–3477.

[4] K.L. Dhumaskar, S.N. Meena, S.C. Ghadi, S.G. Tilve, Graphite catalyzed solvent free synthesis of dihydropyrimidin-2(1H)-ones/thiones and their antidiabetic activity, Bioorg. Med. Chem. Lett. 24 (2014) 2897–2899.

[5] A.A. Bilgin, Z. Ozdemir, H.B. Kandilci, B. Gumusxel, U. Calisx, Synthesis and studies on antidepressant and anticonvulsant activities of some 3-(2-furyl)-pyrazoline derivatives, Eur. J. Med. Chem. 42 (2007) 373–379.

[6] B. Lippert, Cisplatin Chemistry and Biochemistry of a Leading Anticancer Drug, Wiley Interscience, 1999.

[7] M. Arsenijević, M. Milovanović, V. Volarević, D. Canović, N. Arsenijević, T. Soldatović, S. Jovanović, Z.D. Bugarčić, Cytotoxic properties of platinum (IV) and dinuclear platinum (II) complexes and their ligand substitution reactions with guanosine-5'-monophosphate, Trans. Met. Chem. 37 (2012) 481–488.

[8] F.P.T. Hamers, W.H. Gispen, J.P. Neijt, Neurotoxic side-effects of cisplatin, Eur. J. Cancer. 3 (1991) 372–376.

[9] R.W. Schrier, Cancer therapy and renal injury, J. Clin. Invest. 110 (2002) 743–745.

[10] I. Arany, R.L. Safirstein, Cisplatin nephrotoxicity, Semin. Nephrol. 23 (2003) 460–464.

[11] I. Ott, R. Gust, Non platinum metal complexes as anti-cancer drugs, Arch. Pharm. 340 (2007) 117–126.

[12] L. Xie, Z. Luo, Z. Zhao, T. Chen, A mitochondrion-targeting copper complex exhibits potent cytotoxicity against cisplatin-resistant tumor cells through multiple mechanisms of action, Chem. Sci. 5 (2014) 2761–2770.

[13] N. Joksimović, D. Baskić, S. Popović, M. Zarić, M. Kosanić, B. Ranković, T. Stanojković, S.B. Novaković, G. Davidović, Z. Bugarčić, N. Janković, Synthesis, characterization, biological activity, DNA and BSA binding study: novel copper(II) complexes with 2-hydroxy-4-aryl-4-oxo-2-butenoate, Dalton Trans. 45 (2016) 15067–15077.

[14] R. Gust, I. Ott, D. Posselt, K. Sommer, Development of cobalt (3,4-diarylsalen) complexes as tumor therapeutics, J. Med. Chem. 47 (2004) 5837–5846.

[15] S.K. Hadjikakou, N. Hadjiliadis, Antiproliferative and anti-tumor activity of organotin compounds, Coord. Chem. Rev. 253 (2009) 235–249.

[16] M. Arsenijević, M. Milovanović, V. Volarević, A. Djeković, T. Kanjevac, N. Arsenijević, S. Dukic, Ž.D. Bugarčić, Cytotoxicity of gold(III) complexes on A549 human lung carcinoma epithelial cell line, Med. Chem. 8 (2012) 2–8.

[17] D. Lazić, A.N. Arsenijević, R. Puchta, Ž.D. Bugarčić, A. Rilak, DNA binding properties, histidine interaction and cytotoxicity studies of water soluble ruthenium(II) terpyridine complexes, Dalton Trans. 45 (2016) 4633–4646.

[18] F.M. Siu, I.S.W. Lin, K. Yan, C.N. Lok, H.K. Low, T.C.Y. Leung, L.T.C.M. Lam, Anticancer dirhodium(ii,ii) carboxylates as potent inhibitors of ubiquitin- proteasome system, Chem. Sci. 3 (2012) 1785–1793.

[19] X.W. Ni, L.W. Man, T.M. Cheung, W.R. Sun, L.Y. Shu, W.Y. Lam, M.C. Che, C.T. Lau, Osmium(VI) complexes as a new class of potential anti-cancer agents, Chem. Commun. 7 (2011) 2140–2142.

[20] P.M. Abeysinghe, M.M. Harding, Antitumour bis(cyclopentadienyl) metal complexes: titanocene and molybdocene dichloride and derivatives, Dalton Trans. 32 (2007) 3474–3482.

[21] L. He, Y. Li, C.P. Tan, R.R. Ye, M.H. Chen, J.J. Cao, N.L. Ji, Z.W. Mao, Cyclometalated iridium(III) complexes as lysosome-targeted photodynamic anticancer and real-time tracking agents, Chem. Sci. 6 (2015) 5409–5418.

[22] A.R. Kapdi, I.J.S. Fairlamb, Anti-cancer palladium complexes: a focus on PdX2L2, palladacycles and related complexes, Chem. Soc. Rev. 43 (2014) 4751–4777.

[23] J. Petronijević, N. Janković, T.P. Stanojković, N. Joksimović, N.Đ. Grozdanić, M. Vraneš, A. Tot, Z. Bugarčić, Biological evaluation of selected 3,4-dihydro-2(1H)-quinoxalinones and 3,4-dihydro1,4-benzoxazin-2-ones: Molecular docking study, Arch. Pharm. Chem. Life Sci. (2018), https://doi.org/10.1002/ardp.201700308.

[24] J. Petronijević, N. Janković, Z. Bugarčić, Synthesis of quinoxaline-based compounds and their antitumor and antiviral potentials, Mini Rev. Org. Chem. 14 (2017), https://doi.org/10.2174/1570193X14666171201143357.

[25] U. Soumyanarayanan, V.G. Bhat, S.S. Kar, J.A. Mathew, Monastrol mimic Biginelli dihydropyrimidinone derivatives: synthesis, cytotoxicity screening against HepG2 and HeLa cell lines and molecular modeling study, Org. Med. Chem. Lett. 2 (2012) 1–11.

[26] L.M. Ramos, B.C. Guido, C.C. Nobrega, J.R. Corrêa, R.G. Silva, H.C.B. de Oliveira, et al., The Biginelli reaction with an imidazoliumtagged recyclable iron catalyst: kinetics, mechanism, and antitumoral activity, Chem. Eur. J. 19 (2013) 4156–4168.

[27] Z. Ratković, J. Muškinja, A. Burmudžija, B. Ranković, M. Kosanić, G.A. Bogdanović, B. Simović-Marković, A. Nikolić, N. Arsenijević, S. Đorđevic, R.D. Vukićević, Dehydrozingerone based 1-acetyl-5-aryl-4,5-dihydro-1H-pyrazoles: synthesis, characterization and anticancer activity, J. Mol. Struct. 1109 (2016) 82–88.

[28] T.U. Mayer, T.M. Kapoor, S.J. Haggarty, R.W. King, S.L. Schreiber, T.J. Mitchison, Small molecule inhibitor of mitotic spindle bipolarity identified in a phenotype-based screen, Science 286 (1999) 971–974.

[29] D. Russowsky, R.F.S. Canto, S.A.A. Sanches, M.G.M. D'oca, A. de Fatima, R.A. Pilli, et al., Synthesis and differential antiproliferative activity of Biginelli compounds against cancer cell lines: monastrol, oxo-monastrol and oxygenated analogues, Bioorg. Chem. 34 (2006) 173–182.

[30] K. Zhang, W. Liu, Investigation of the electrochemical interaction behavior of DNA with 5-fluorouracil derivatives, Int. J. Electrochem. Sci. 6 (2011) 1669–1678.

[31] S.F. Sun, B. Zhou, H.N. Hou, Y. Liu, G.Y. Xiang, Studies on the interaction between Oxaprozin-E and bovine serum albumin by spectroscopic methods, Int. J. Biol. Macromol. 39 (2006) 197–200.

[32] M.W. Roomi, J.C. Monterrey, T. Kalinovsky, M. Rath, A. Niedzwiecki, In vitro modulation of MMP-2 and MMP-9 in human cervical and ovarian cancer cell lines by cytokines, inducers and inhibitors, Oncol. Rep. 23 (2010) 605–614.

[33] A.H. Baker, S.J. George, A.B. Zaltsman, G. Murphy, A.C. Newby, Inhibition of invasion and induction of apoptotic cell death of cancer cell lines by overexpression of TIMP-3, Br. J. Cancer 79 (1999) 1347–1355.

[34] G. Shishodia, S. Shukla, Y. Srivastava, S. Shashank Masaldan, S. Mehta, S. Bhambhani, R. Sharma, B Chandra Mehrotra, A Chandra Das, Bhart, Alterations in microRNAs miR-21 and let-7a correlate with aberrant STAT3 signaling and downstream effects during cervical carcinogenesis, Mol. Cancer 14 (2015) 116–129.

[35] J. Hu, S. Ni, Y. Cao, T. Zhang, T. Wu, X. Yin, Y. Lang, H. Lu, The angiogenic effect of microRNA-21 targeting TIMP3 through the regulation of MMP2 and MMP9, PLoS ONE 11 (2) (2016).

[36] L.E. Buscaglia, Y. Li, Apoptosis and the target genes of microRNA-21, Chin. J. Cancer. 30 (6) (2011) 371–380.

[37] N. Janković, Z. Bugarčić, S. Marković, Double catalytic effect of (PhNH3)2CuCl4 in a novel, highly efficient synthesis of 2-oxo and thioxo-1,2,3,4-tetrahydropyrimidines, J. Serb. Chem. Soc. 80 (2015) 1–13.

[38] J. Muškinja, N. Janković, Z. Ratković, G. Bogdanović, Z. Bugarčić, Vanillic aldehydes for the one-pot synthesis of novel 2-oxo-1,2,3,4-tetrahydropyrimidines, Mol. Divers. 20 (2016) 591–604.

[39] M. Gavrilović, N. Janković, L.J. Joksović, J. Petronijević, N. Joksimović, Z. Bugarčić, Water ultrasound-assisted oxidation of 2-oxo-1,2,3,4-tetrahydropyrimidines and benzylic acid salts, Environ. Chem. Lett. (2018), https://doi.org/10.1007/s10311-018-0766-z.

[40] N. Janković, S. Stefanović, J. Petronijević, N. Joksimović, S.B. Novaković, G.A. Bogdanović, J. Muškinja, M. Vraneš, Z. Ratković, Z. Bugarčić, ACS Sustain. Chem. Eng. 6 (10) (2018) 13358–13366.

[41] A. Pereira, M. Bester, P. Soundy, Z. Apostolides, Anti-proliferative properties of commercial Pelargonium sidoides tincture, with cell-cycle G0/G1 arrest and apoptosis in Jurkat leukaemia cells, Pharm Biol. 54 (2016) 1831–1840.

[42] M. Molinari, Cell cycle checkpoints and their inactivation in human cancer, Cell Prolif. 33 (2000) 261–274.

[43] K.A. Schafer, The cell cycle: a review, Vet. Pathol. 35 (1998) 461–478.

[44] B.B. Zhou, S.J. Elledge, The DNA damage response: putting checkpoints in perspective, Nature 408 (2000) 433–439.

[45] S.S. Margolis, J.A. Perry, D.H. Weitzel, C.D. Freel, M. Yoshida, T.A. Haystead, S. Kornbluth, A role for PP1 in the Cdc2/Cyclin B-mediated positive feedback activation of Cdc25, Mol. Biol. Cell 17 (2006) 1779–1789.

[46] E.A. Slee, M.T. Harte, R.M. Kluck, B.B. Wolf, C.A. Casiano, D.D. Newmeyer, H.G. Wang, J.C. Reed, D.W. Nicholson, E.S. Alnemri, D.R. Green, S.J. Martin, Ordering the cytochrome c-initiated caspase cascade: hierarchical activation of caspases-2, -3, -6, -7,-8, and -10 in a caspase-9-dependent manner, J. Cell Biol. 144 (1999) 281–292.

[47] A.B. Parrish, C.D. Freel, S. Kornbluth, Cellular mechanisms controlling caspase activation and function, Cold. Spring. Harb. Perspect. Biol. 5 (2013) pii:a008672.

[48] R.S. Kerbel, Antiangiogenic therapy: a universal chemosensitization strategy for cancer? Science 312 (2006) 1171–1175.

[49] N. Petrovic, S. Ergun, miRNAs as potential treatment targets and treatment options in cancer, Mol. Diagn. Ther. (2018), https://doi.org/10.1007/s40291-017-0314-8.

[50] F. Liu, T. Shimakami, K. Murai, T. Shirasaki, M. Funaki, M. Honda, S. Murakami, M. Yi, H. Tang, S. Kaneko, Efficient suppression of hepatitis C virus replication by combination treatment with miR-122 antagonism and direct-acting antivirals in cell culture systems, Sci. Rep. 6 (2016) 30939.

[51] R. Devulapally, T.V. Sekar, R. Paulmurugan, Formulation of Anti-miR-21 and 4-Hydroxytamoxifen co-loaded biodegradable polymer nanoparticles and their anti-proliferative effect on breast cancer cells, Mol. Pharm. 12 (2015) 2080–2092.

[52] Y. Todo, H. Watari, Concurrent chemoradiotherapy for cervical cancer: background including evidence-based data, pitfalls of the data, limitation of treatment in certain groups, Chin. J. Cancer Res. 28 (2016) 221–227.

[53] N.M.R. Martins, S. Anbu, K.T. Mahmudov, R. Ravishankaran, M.F.C.G. da Silva, L.M.D.R.S. Martins, A.A. Karande, A.J.L. Pombeiro, DNA and BSA binding and cytotoxic properties of copper (II) and iron (III) complexes with arylhydrazone of ehtyl 2-cyanoacetate or formazan ligands, New J. Chem. 41 (2017) 4076–4086.

[54] F. Arjmand, S. Parveen, M. Afzal, M. Shahid, Synthesis, characterization, biological studies (DNA binding, cleavage, antibacterial and topoisomerase I) and molecular docking of copper (II) benzimidazole complexes, J. Photochem. Photobiol. B. 114 (2012) 15–26.

[55] X. Zhou, L. Ji, X. Ran, B. Su, Q. Ji, C. Pan, J. Weng, C. Ma, C. Hao, D. Zhang, D. Hu, Prevalence of obesity and its influence on achievement of cardiometabolic therapeutic goals in chinese type 2 diabetes patients: an analysis of the nationwide, cross-sectional 3B study, PLoS One 11 (2016).

[56] J. Trifunović, V. Borčić, S. Vukmirović, S. Goločorbin-Kon, M. Mikov, Retention data of bile acids and their oxo derivatives in characterization of pharmacokinetic properties and in silico ADME modeling, Eur J. Pharm. Sci. 92 (2016) 194–202.

[57] A. Spurgand, S.R. Waldvogel, High-yielding cleavage of (aryloxy)acetates, Eur. J.

Org. Chem. 2 (2007) 337–342.
[58] Agilent,, CrysAlis PRO, Agilent Technologies, Yarnton, Oxfordshire, England, 2013.
[59] G.M. Sheldrick, A short history of SHELX, Acta Cryst. Sect. A 64 (2008) 112–122.
[60] C.F. Macrae, P.R. Edgington, P. McCabe, E. Pidcock, G.P. Shields, R. Taylor, M. Towler, J. van de Streek, Mercury: visualization and analysis of crystal structures, J. Appl. Cryst. 39 (2006) 453–457.
[61] L.J. Farrugia, WinGX suite for small-molecule single-crystal crystallography, J. Appl. Cryst. 32 (1999) 837–838.
[62] A.L. Spek, Single-crystal structure validation with the program PLATON, J. Appl. Crystallogr. 36 (2003) 7–13.
[63] M. Nardelli, PARST95 – an update to PARST: a system of Fortran routines for calculating molecular structure parameters from the results of crystal structure analyses, J. Appl. Cryst. 28 (1995) 659.
[64] T. Mosmann, Rapid colorimetric assay for cellular growth and survival: Application to proliferation and cytotoxicity assays, J. Immunol. Methods 65 (1983) 55–63.
[65] M. Ohno, T. Abe, Rapid colorimetric assay for the quantification of leukemia inhibitory factor (LIF) and interleukin-6 (IL-6), J. Immunol. Methods 145 (1991) 199–203.
[66] M.G. Ormerod, Flow Cytometry. A Practical Approach, Oxford University Press, 2000.
[67] E. Aranda, G.I. Owen, A semi-quantitative assay to screen for angiogenic compounds and compounds with angiogenic potential using the EA.hy926 endothelial cell line, Biol. Res. 42 (2009) 377–389.
[68] C. My Du, K. Valko, C. Bevan, D. Reynolds, M. Abraham, Rapid gradient RP-HPLC method for lipophilicity determination: a solvation equation based comparison with isocratic methods, Anal. Chem. 70 (1998) 4228–4234.
[69] D.S. Cao, Q.S. Xu, Q.N. Hu, Y.Z. Liang, ChemoPy: freely available python package for computational biology and chemoinformatics, Bioinformatics 29 (2013) 1092–1094.
[70] Schrödinger Suite 2015, Protein Preparation Wizard, Schrödinger, LLC, New York, NY.
[71] M. Rostkowski, M. Olsson, C. Sondergaard, J. Jensen, Graphical analysis of pH-dependent properties of proteins predicted using PROPKA, BMC Struct. Biol. 11 (2011) 1–6.
[72] W.L. Jorgensen, J. Tirado-Rives, Potential energy functions for atomic-level simulations of water and organic and biomolecular systems, Proc. Natl. Acad. Sci. USA 102 (2005) 6665–6670.
[73] Schrödinger Suite 2015, Glide, Schrödinger, LLC, New York, NY.